IX CONGRESSO BRASILEIRO DE
ENGENHARIA E CIÊNCIAS TÉRMICAS

9th BRAZILIAN CONGRESS OF THERMAL
ENGINEERING AND SCIENCES

Paper CIT02-0393

A FINITE ELEMENT ANALYSIS OF GAS-LUBRICATED HERRINGBONE GROOVE JOURNAL BEARINGS

Marco Túlio C. Faria
Universidade Federal de Minas Gerais
Departamento de Engenharia Mecânica
Av. Antônio Carlos, 6627
Belo Horizonte, MG – 31270-901- Brasil
mtfaria@dedalus.lcc.ufmg.br

Abstract. *A finite element analysis is carried out to investigate the behavior of gas lubricated herringbone groove journal bearings operating at high speeds. A special finite element procedure, based on the Galerkin weighted residual method with a new class of high-order shape functions, is implemented to solve the Reynolds equation for compressible fluids in journal bearings. A linearized perturbation procedure is performed on the Reynolds equation to render the zeroth- and first-order lubrication equations for grooved journal bearings. These zeroth- and first-order lubrication equations permit the prediction of some bearing static and dynamic performance characteristics, such as load capacity and dynamic force coefficients. Curves of performance characteristics show the influence of high speeds on the behavior of gas grooved journal bearings.*

Keywords*. Gas bearings, journal bearings, herringbone grooves, grooved bearings, upwind techniques*

1. Introduction

Nowadays, gas bearings are finding numerous industrial applications, such as computer storage devices, precision equipment, guidance mechanisms, lightweight rotating machinery and electronics (Pan, 1990). Fixed and non-fixed bearing geometries have been widely employed in journal bearings for industrial machinery and equipment that require an oil-free environment and very low friction. Advances in gas bearing technology rely heavily on the development of numerical tools capable of predicting the bearing performance under several operating conditions. Preliminary bearing performance analysis is a very important stage in the design of gas bearings, providing useful data for selection of an appropriate bearing configuration for a given industrial application.

One of the best combinations of cost and performance among self-acting gas journal bearing designs is the herringbone groove journal bearing (HGJB) (Cunningham et all, 1969). Gas HGJBs have been successfully used in lightweight rotating machinery and high-precision equipment due to their high stiffness, good dynamic stability against self-excited whirl and low manufacturing costs. Some important applications of gas HGJBs are automotive turbochargers and rotating parts of video and audio equipment. The technical literature lacks both numerical and experimental data about the static and dynamic performance of gas HGJBs

Due to its capability of representing complex geometries and associated boundary conditions, the finite element method (FEM) has been recently used to devise some models for gas HGJBs. Finite element procedures for gas HGJBs are generally based on either the Galerkin (Kinouchi et all, 1996) or the Petrov-Galerkin (Bonneau and Absi, 1994) weighted residual method. Schemes based on the Galerkin method usually require fine meshes to provide stable numerical solutions for high speed gas bearings (Faria and San Andrés, 2000). Schemes based on the Petrov-Galerkin method are able to provide efficient and stable FEM procedures for high speed gas bearings, but require special numerical integration procedures to deal with the advection flow terms of the Reynolds equations and generally introduce numerical artificial diffusion into the solution (Faria, 1999).

In order to analyze some static and dynamic performance characteristics of gas HGJBs operating at high speeds, an efficient and accurate finite element procedure, founded on the Galerkin weighted residual method with a novel class of high order shape functions, is employed (Faria, 2001). The high order shape functions are derived from the Reynolds equation within an element domain (Faria and San Andrés, 2000). The high order finite element procedure eliminates not only the need of fine meshes but also does not introduce artificial diffusion into the solution of the Reynolds equation for compressible fluids. Furthermore, a linearized perturbation procedure is applied on the Reynolds equation to render the zeroth- and first-order lubrication equations, which permit the computation of the bearing load capacity and the dynamic force coefficients, respectively. Bearing load-capacity and frequency-dependent force coefficients are predicted for gas HGJBS operating at high speeds. The analysis shows the effects of high speeds on the performance characteristics of gas HGJBs.

2. Parameters and governing equations for a Gas HGJB

Figures (1) e (2) depict the geometry and parameters describing a gas-lubricated herringbone groove journal bearing (HGJB). The bearing geometry includes the groove angle β, the ridge bearing clearance c, the groove depth c_g, the ridge width w_r and the groove width w_g. The journal rotational speed is denoted by Ω. Journal eccentricities in the vertical and horizontal directions are expressed as e_X and e_Y, respectively. The eccentricity ratio is defined as $\varepsilon = e/c$, where $e^2=e_X^2+e_Y^2$. The bearing attitude angle, ϕ, is defined as $\phi = a\tan(-F_Y/F_X)$, where F_Y and F_X are the horizontal and vertical components, respectively, of the bearing reaction force F. Two useful parameters for grooved bearings are the groove width ratio, $\alpha_g = w_g/(w_g + w_r)$, and the groove length ratio, $l_g = L_g / L$, where L_g is the extent of the grooved region in the axial direction and L is the bearing length. l_g=1 for the fully grooved bearing shown in Fig. (2) and l_g<1 for partially grooved journal bearings. The partially grooved bearing has a circumferential land centrally located along the bearing length. (X,Y,Z) is an inertial reference frame, and (x,y,z) is a rotating coordinate system attached to the journal, where $x=R\theta$ and R is the bearing radius. The circumferential coordinate Φ is fixed to the bearing housing, while the coordinate θ rotates with the journal ($\Phi = \theta + \Omega t$). The bearing motion is described in relation to the coordinate system attached to the grooved member (Faria, 2001).

The Reynolds equation for an isothermal, isoviscous, ideal gas in the rotating coordinate system (x,y,z) is written in the following form (Hamrock, 1994):

$$\frac{1}{R^2}\frac{\partial}{\partial\theta}\left(\frac{ph^3}{12\mu}\frac{\partial p}{\partial\theta}\right)+\frac{\partial}{\partial z}\left(\frac{ph^3}{12\mu}\frac{\partial p}{\partial z}\right)=\frac{1}{2}\frac{U}{R}\frac{\partial(ph)}{\partial\theta}+\frac{\partial(ph)}{\partial t} \tag{1}$$

on the flow domain $0 \le \theta \le 2\pi$, $\frac{-L}{2} \le z \le \frac{L}{2}$. U represents the journal surface speed, p is the pressure field and μ is the fluid viscosity. For stationary grooves (smooth journal) $U = \Omega R$, while for rotating grooves (grooved journal) $U = -\Omega R$. The bearing sides are at ambient pressure p_a and the pressure is periodic in the circumferential direction. Expressions for the film thickness h at the ridge and groove of a HGJB are given as.

$$h = c + e_X(t)\cos(\theta + \Omega.t) + e_Y(t)\sin(\theta + \Omega.t) \tag{2}$$

$$h = c + c_g + e_X(t)\cos(\theta + \Omega.t) + e_Y(t)\sin(\theta + \Omega.t) \tag{3}$$

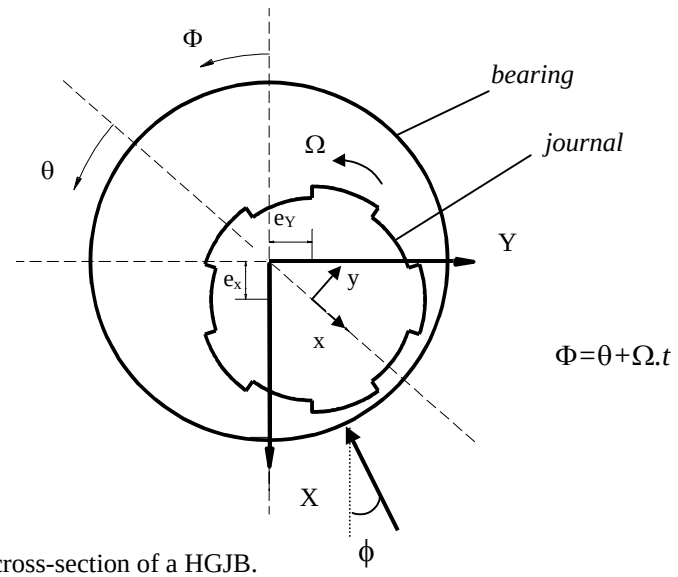

Figure 1. Schematic view of a cross-section of a HGJB.

3. Linearized Perturbation Procedure

A perturbation analysis is performed to obtain the zeroth- and first-order lubrication equations for computation of the bearing load-capacity and dynamic force coefficients, respectively. A journal equilibrium position described by (e_{Xo},e_{Yo}) is perturbed by small amplitude journal motions $(\Delta e_X, \Delta e_Y)$ with an excitation frequency (ω). The film thickness is then given as

$$h = h_o + (\Delta e_X h_X + \Delta e_Y h_Y)e^{i\omega t} = h_o + \Delta e_\sigma h_\sigma e^{i\omega t}; \quad (\sigma = X, Y;\ i = \sqrt{-1}) \tag{4}$$

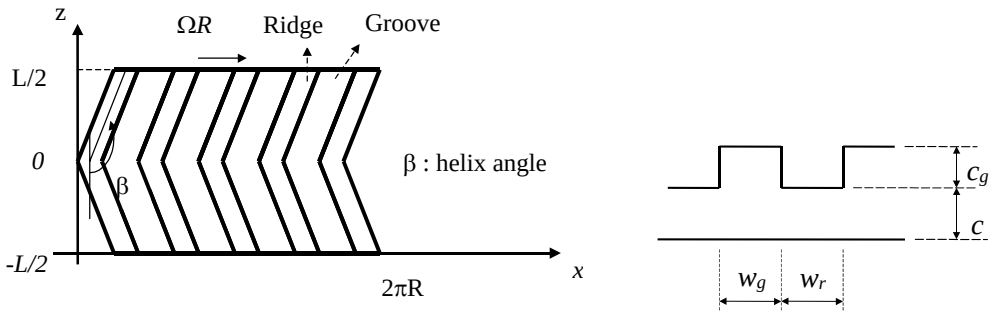

(a) Unwrapped bearing geometry (c) Detail of a ridge-groove pair

Figure 2. Details of a HGJB geometry.

where $h_X = cos(\theta + \Omega.t)$, $h_Y = sin(\theta + \Omega.t)$ and the zeroth-order film thickness is $h_o = c + e_{X_o} h_X + e_{Y_o} h_Y$ or $h_o = c + c_g + e_{X_o} h_X + e_{Y_o} h_Y$. It is assumed that the periodic perturbations on the film thickness cause the same type of perturbation on the pressure field, which is written as

$$p(\theta, z, t) = p_o(\theta, z, t) + (\Delta e_X p_X + \Delta e_Y p_Y) e^{i\omega t} = p_o + \Delta e_\sigma p_\sigma e^{i\omega t}; \sigma = X, Y \tag{5}$$

where p_o and $\{ p_\sigma \}_{\sigma = X,Y}$ represent the zeroth- and first-order pressure fields, respectively.

By substituting equations (4) and (5) into the governing equation (1), the zeroth- and first-order lubrication equations are obtained in the following form:

$$\frac{1}{R^2}\frac{\partial}{\partial\theta}\left(\frac{p_o h_o^3}{12\mu}\frac{\partial p_o}{\partial\theta}\right) + \frac{\partial}{\partial z}\left(\frac{p_o h_o^3}{12\mu}\frac{\partial p_o}{\partial z}\right) = \frac{1}{2}\frac{U}{R}\frac{\partial(p_o h_o)}{\partial\theta} + \frac{\partial}{\partial t}(p_o h_o) \tag{6}$$

$$\frac{1}{R^2}\frac{\partial}{\partial\theta}\left(\frac{3p_o h_o^2 h_\sigma}{12\mu}\frac{\partial p_o}{\partial\theta} + \frac{h_o^3}{12\mu}\frac{\partial(p_\sigma p_o)}{\partial\theta}\right) + \frac{\partial}{\partial z}\left(\frac{3p_o h_o^2 h_\sigma}{12\mu}\frac{\partial p_o}{\partial z} + \frac{h_o^3}{12\mu}\frac{\partial(p_\sigma p_o)}{\partial z}\right) =$$
$$\frac{1}{2}\frac{U}{R}\left[\frac{\partial(h_o p_\sigma)}{\partial\theta} + \frac{\partial(p_o h_\sigma)}{\partial\theta}\right] + i\omega(h_o p_\sigma + p_o h_\sigma) + \frac{\partial(p_o h_\sigma)}{\partial t} + \frac{\partial(p_\sigma h_o)}{\partial t} \tag{7}$$

Smooth and grooved journals are usually employed in HGJB designs. For simplicity, this work deals with a finite element procedure developed for bearings with a smooth rotating journal (Faria, 2001).

4. Finite element high-order scheme

The zeroth- and first order pressure fields are interpolated by using a new class of high-order shape functions $\{ \psi_j^e \}_{j=1,2,3,4}$, derived from an approximate solution to the non-linear Reynolds equation within an element (*e*). The steady-state two-dimensional Reynolds equation for a four-node element (*e*), written in relation to an arbitrary two-dimensional coordinate system (*x*,*y*), is expressed as

$$\frac{\partial}{\partial x}\left(\frac{p_e h_e^3}{12\mu}\frac{\partial p_e}{\partial x}\right) + \frac{\partial}{\partial y}\left(\frac{p_e h_e^3}{12\mu}\frac{\partial p_e}{\partial y}\right) = \frac{u}{2}\frac{\partial}{\partial x}(p_e h_e) \tag{8}$$

The nodal values of pressure within element (*e*) are given by p_i^e, *i*=1,2,3,4. Over an element domain, $\left(\frac{p_e h_e^3}{12\mu}\right)$ e $u.h_e$ are computed for meaningful averaged values of pressure p_e and film thickness h_e within (*e*) (Faria, 2001). Hence, Eq.(8) is re-written as

$$\frac{\partial^2 p_e}{\partial x^2} + \frac{\partial^2 p_e}{\partial y^2} = \nu\frac{\partial p_e}{\partial x} \tag{9}$$

where $\nu = \dfrac{6\mu u}{p_e h_e^2}$. The linear partial differential equation (9) can be solved by separation of variables, assuming that the constant generated by the separation principle is zero (Faria, 2001). Hence, the solution has the form $p_e = (Ae^{\nu x} + B).(C.y + D)$, where *A,B,C,* e *D* are constants.

Figure (3) depicts the transformation from the local coordinate system (*x,y*) to the natural coordinate system (ξ,η) for an element (*e*). The "exact" or high-order shape functions, for an element domain Ω_e in its natural coordinate system (ξ,η), are then expressed as

$$\psi_1^e = \frac{1}{2}(1-\eta)\left(\frac{e^{\lambda_e} - e^{\lambda_e \xi}}{e^{\lambda_e} - e^{-\lambda_e}}\right) \tag{10}$$

$$\psi_2^e = \frac{1}{2}(1-\eta)\left(\frac{e^{\lambda_e \xi} - e^{-\lambda_e}}{e^{\lambda_e} - e^{-\lambda_e}}\right) \tag{11}$$

$$\psi_3^e = \frac{1}{2}(1+\eta)\left(\frac{e^{\lambda_e \xi} - e^{-\lambda_e}}{e^{\lambda_e} - e^{-\lambda_e}}\right) \tag{12}$$

$$\psi_4^e = \frac{1}{2}(1+\eta)\left(\frac{e^{\lambda_e} - e^{\lambda_e \xi}}{e^{\lambda_e} - e^{-\lambda_e}}\right) \tag{13}$$

where $\lambda_e = \dfrac{6\mu u L_e}{p_e h_e^2}$ is a local speed or Peclet number. L_e is the averaged element length computed in the circumferential direction. For the limit case, $\lambda_e \to 0$, the "exact" shape functions become the bilinear interpolation functions (Bathe, 1982). The "exact" shape functions are of higher order than those of polynomials widely used in the FEM. The upwinding effect is intrinsically contained in the high-order functions without resort to special schemes for the advection terms. No artificial viscosity is therefore introduced into the solution.

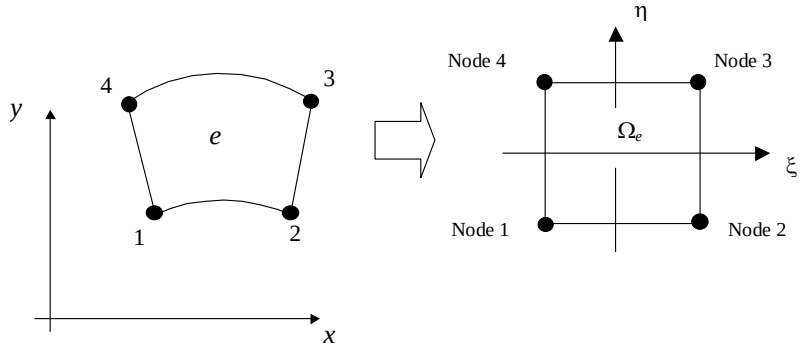

Figure 3. Transformation from local coordinates to natural coordinates for element (*e*).

5. Finite element lubrication equations

The Galerkin weighted residual method is used to derive the zeroth- and first-order lubrication equations for a finite element domain (Bathe, 1982). Four-node isoparametric finite elements are employed in the discretization of the thin gas flow domain and the zeroth- and first-orde pressure fields are interpolated using the high-order shape functions; $p_o^e = \sum_{i=1}^{4} \psi_i^e p_{oi}^e$ and $p_\sigma^e = \sum_{i=1}^{4} \psi_i^e p_{\sigma_i}^e$. Equation (6) leads to the following system of finite element equations, which allow the computation of the zeroth-order stationary pressure field within an element (*e*).

$$k_{ji}^e p_{oi}^e = q_j^e \quad ; i,j=1,2,3,4 \tag{14}$$

where

$$k_{ji}^e = \iint_{\Omega_e} \left(\frac{p_o h_o^3}{12\mu} \left(\frac{1}{R^2} \frac{\partial \psi_i^e}{\partial \theta} \frac{\partial \psi_j^e}{\partial \theta} + \frac{\partial \psi_i^e}{\partial z} \frac{\partial \psi_j^e}{\partial z} \right) - \frac{U}{2} h_o \frac{\partial \psi_j^e}{R \partial \theta} \psi_i^e \right) . d\Omega_e \tag{15}$$

$$q_j^e = -\oint_{\Gamma_e} \psi_j^e \dot{m}_n^e d\Gamma_e \tag{16}$$

k_{ji}^e represent the coefficients of the elementary fluidity matrix; q_j^e represents the nodal flux through the element boundary Γ_e. The normal mass flow rate outward the element boundary is given by $\dot{m}_n^e$. The method of successive substitutions (Dahlquist and Björck, 1974) is employed to solve the global non-linear Reynolds equation. The initial guess for pressure is the ambient pressure. The iterative process ends when $|F_{new} - F_{old}| \le 0.001$, where F_{new} is the bearing load capacity computed at iteration (*n*) and F_{old} is the force at the previous iteration (*n-1*).

Similarly, the linear stationary first-order lubrication equations are obtained from Eq. (7).

$$k_{\sigma_{ji}}^e p_{\sigma_i}^e = f_{\sigma_j}^e + q_{\sigma_j}^e \;;\; i,j=1,2,3,4 \tag{17}$$

where

$$k_{\sigma_{ji}}^e = \iint_{\Omega_e} \left\{ \frac{h_o^3}{12\mu} \left(\frac{1}{R^2} \frac{\partial p_o}{\partial \theta} \frac{\partial \psi_j^e}{\partial \theta} + \frac{\partial p_o}{\partial z} \frac{\partial \psi_j^e}{\partial z} \right) \psi_i^e + \frac{h_o^3 p_o}{12\mu} \left(\frac{1}{R^2} \frac{\partial \psi_i^e}{\partial \theta} \frac{\partial \psi_j^e}{\partial \theta} + \frac{\partial \psi_i^e}{\partial z} \frac{\partial \psi_j^e}{\partial z} \right) - \frac{U}{2} \frac{h_o}{R} \psi_i^e \frac{\partial \psi_j^e}{\partial \theta} + i\omega h_o \psi_j^e \psi_i^e \right\} d\Omega_e \tag{18}$$

$$f_{\sigma_j}^e = \iint_{\Omega_e} \left\{ \frac{-3 p_o h_o^2 h_\sigma}{12\mu} \left(\frac{1}{R^2} \frac{\partial p_o}{\partial \theta} \frac{\partial \psi_j^e}{\partial \theta} + \frac{\partial p_o}{\partial z} \frac{\partial \psi_j^e}{\partial z} \right) + \frac{U}{2} p_o \frac{h_\sigma}{R} \frac{\partial \psi_j^e}{\partial \theta} - i\omega . p_o h_\sigma \psi_j^e \right\} . d\Omega_e \tag{19}$$

$$q_{\sigma_j}^e = -\oint_{\Gamma_e} \psi_j^e \dot{m}_{\sigma n}^e d\Gamma_e \tag{20}$$

where $k_{\sigma ji}^e$ represents the complex first-order fluidity matrix; $f_{\sigma_j}^e$ represents the right-hand side first-order flux vector within element (*e*); $q_{\sigma_j}^e$ represents the first-order nodal flux through the element boundary; $\dot{m}_{\sigma n}^e$ represents the first-order mass flow rate through the element boundary.

6. Bearing reaction force and dynamic force coefficients

The zeroth- and first-order pressure fields are integrated over the bearing domain to generate the fluid film reaction forces $\{F_{\sigma_o}\}_{\sigma=X,Y}$ and dynamic complex impedances $\{Z_{\sigma\beta_o}\}_{\beta,\sigma=X,Y}$. The fluid film bearing reaction forces acting on the journal for a stationary position (e_{X_o}, e_{Y_o}) are given as

$$F_{\sigma_o} = \int_0^L \int_0^{2\pi} (p_o - p_{ref}) h_\sigma R.d\theta.dz \;;\; \sigma = X,Y \tag{21}$$

where p_{ref} is the reference pressure (p_a).

The bearing dynamic coefficients associated with the stiffness $\{K_{\sigma\beta}\}_{\beta,\sigma=X,Y}$ and damping $\{C_{\sigma\beta}\}_{\beta,\sigma=X,Y}$ are calculated from the complex impedances in the following form

$$Z_{\sigma\beta} = K_{\sigma\beta} + i\omega C_{\sigma\beta} = -\int_0^L \int_0^{2\pi} p_\beta h_\sigma R.d\theta.dz \;;\; \beta,\sigma = X,Y \tag{22}$$

or

$$\begin{bmatrix} K_{XX} & K_{XY} \\ K_{YX} & K_{YY} \end{bmatrix} + i.\omega . \begin{bmatrix} C_{XX} & C_{XY} \\ C_{YX} & C_{YY} \end{bmatrix} = -\int_0^L \int_0^{2\pi} \begin{bmatrix} p_X h_X & p_Y h_X \\ p_X h_Y & p_Y h_Y \end{bmatrix} .R.d\theta.dz \,. \tag{23}$$

7. Numerical results

Firstly, the accuracy of the high-order finite element procedure is evaluated by comparing the computed finite element predictions for dynamic force coefficients with results available in the technical literature for gas lubricated plain journal bearings. Secondly, some performance characteristics of a gas HGJB are evaluated at concentric and eccentric journal positions.

7.1. Validation

The high-order finite element scheme is evaluated for an air-lubricated unloaded plain journal bearing given by Dimofte and Keith (1998). The bearing parameters are shown in Tab. (1). Predictions obtained by the high-order FEM

scheme are computed for a mesh with 110 elements (11 circumferential elements and 10 axial elements). Figure (4) and Figure (5) depict the comparative results for direct and cross-coupled synchronous (ω = Ω) stiffness and damping coefficients versus the bearing number ($\Lambda = (6\mu\Omega R^2)/(p_a c^2)$). Solid lines indicate the high-order FEM predictions while dashed lines indicate the results presented by Dimofte and Keith. Those figures show the good agreement between the finite element predictions for force coefficients and the results presented in the literature. The normalized coefficients are computed as $\overline{K}_{ij} = \dfrac{K_{ij}}{(p_a LD/c)}$ and $\overline{C}_{ij} = \dfrac{C_{ij}}{(p_a LD/c\Omega)}$, $i,j=x,y$.

Table (1). Plain gas journal bearing parameters for validation of the high-order FEM scheme.

L = 0.05 m	c = 5 μm	p_a = 0.101 MPa
D = 0.05 m	μ = 1.9x10^{-6} Pa.s	ε_y = 0.01
	ρ = 1.32 kg/m^3	ε_x = 0.01

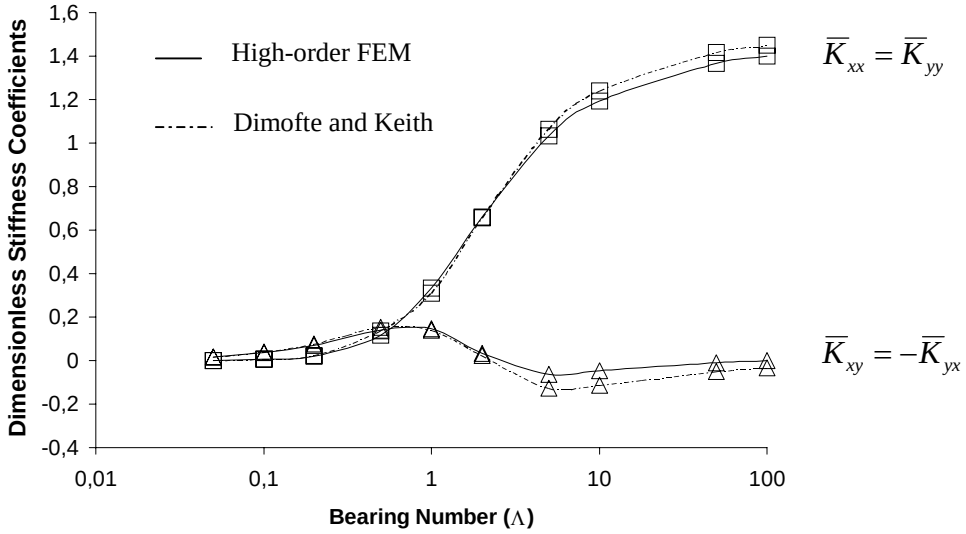

Figure (4). Direct and cross-coupled dimensionless stiffness coefficients versus bearing number for a concentric plain gas journal bearing.

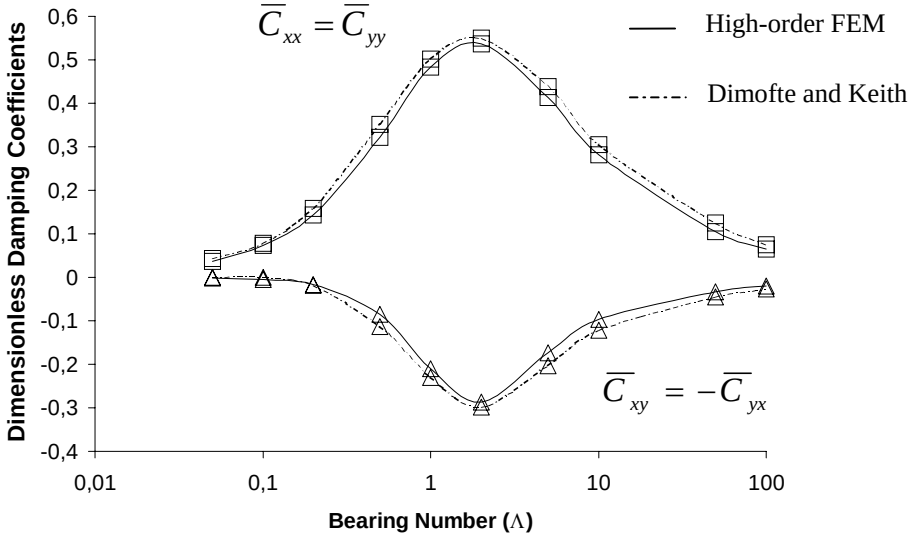

Figure (5). Direct and cross-coupled dimensionless damping coefficients versus bearing number for a concentric plain gas journal bearing.

7.2. Analysis of a gas HGJB

Performance characteristics of a gas HGJB, whose parameters are shown in Tab. (2), are evaluated at concentric and eccentric operating conditions. Rotating machines using gas HGJBs usually operate under light loads. However, the development of lightweight rotating machines operating under stringent conditions has demanded the investigation of gas journal bearings operating at off-centered positions.

Table (2). Baseline parameters of a gas HGJB.

smooth member rotates (journal)		
D = 0.04 m	β = 30°	p_{ref} = 0.10 MPa
L = 0.04 m	α_g = 0.5	ρ =1.32 kg/m^3
c =10 μm	N_g = 4	Ω = 32000 rpm (Λ =15.3)
c_g = 14 μm	μ = 1.9x10^{-5} Pa.s	l_g = 1
Mesh: 784 elements (56 circumferential x 14 axial elements)		

Figure (6) depicts the predictions of the synchronous ($\omega = \Omega$) direct ($\overline{K}_{XX}, \overline{K}_{YY}$) and cross-coupled ($\overline{K}_{XY}, \overline{K}_{YX}$) stiffness coefficients obtained for increasing values of bearing number (Λ). The dimensionless coefficients are computed at concentric operating conditions. The normalization is performed by using $\overline{K}_{ij} = K_{ij}.c/p_a LD$, $i,j=X,Y$. Stiffness coefficients tend towards asymptotic values at large bearing numbers.

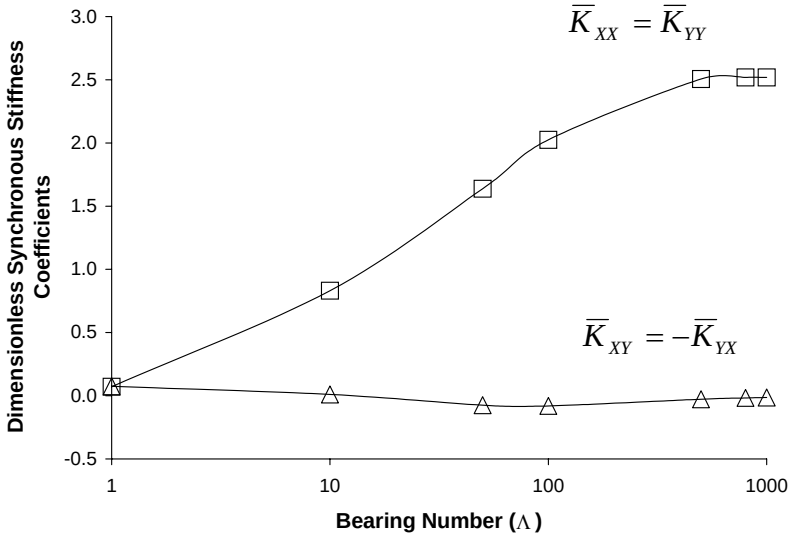

Figure (6). Dimensionless synchronous stiffness coefficients versus bearing number for a centered gas HGJB.

To show the effects of speed and fluid compressibility on the behavior of gas lubricated HGJBs operating at eccentric position ($\varepsilon_X \geq 0, \varepsilon_Y = 0$), bearing load capacity, attitude angles and stiffness coefficients are computed at moderate (Λ = 15.3), high (Λ = 100) and very high (Λ = 300) rotating speeds. Figure (7) and Figure (8) depict the predictions of dimensionless load capacity and respective attitude angles versus the journal eccentricity ratio, respectively, for the gas HGJB given in Tab. (2). The dimensionless bearing load capacity is obtained by dividing the load capacity by ($p_a.L.D$). From low to moderate bearing numbers ($15.3 \leq \Lambda \leq 100$), there is a considerable increase in load capacity, however for $\Lambda > 100$ the load capacity tends to an asymptotic value. For high Λ, the gas lubricating film is governed completely by the compressibility effects.

Finally, Figure (9) and Figure (10) show the dimensionless direct and cross-coupled synchronous stiffness coefficients, respectively, versus eccentricity ratio. Direct stiffness coefficients ($\overline{K}_{XX}, \overline{K}_{YY}$) increase as either Λ or ε increases. For $\varepsilon < 0.4$ the cross-coupled stiffness coefficients are antisymmetric ($\overline{K}_{XY} = -\overline{K}_{YX}$) and remain practically unchanged with increasing ε. For large eccentricities, $\varepsilon > 0.4$, $\overline{K}_{XY}$ and $\overline{K}_{YX}$ are negative and increase as ε increases.

The fluid inertia effects are not taken into account in the analysis. Flow turbulence and fluid inertia effects are expected to have an secondary effect in the computation of the load capacity and dynamic force coefficients of grooved journal bearings lubricated with a low viscosity fluid (Constantinescu and Dimofte, 1987; van der Stegen, 1997), however, in the time-transient analysis, at large Reynolds number, these effects could be significant.

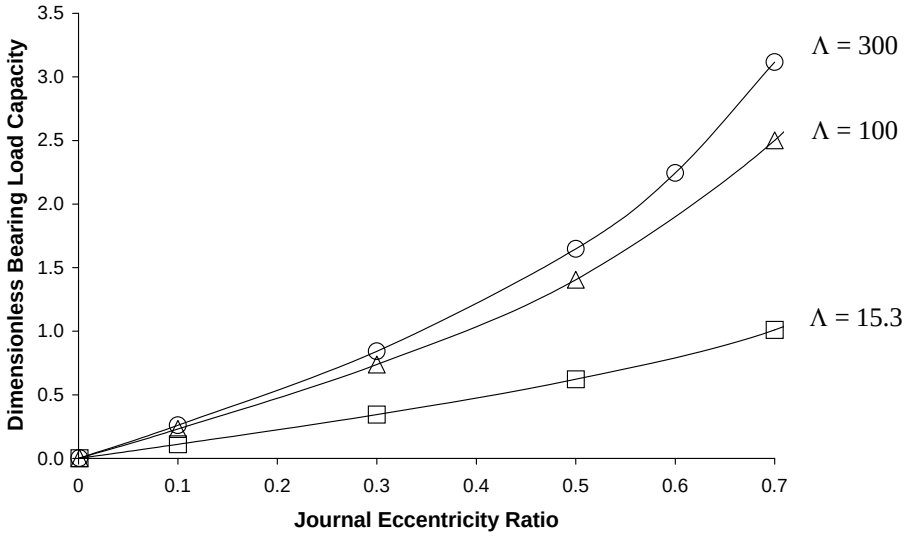

Figure (7). Dimensionless bearing load capacity versus eccentricity ratio for a gas HGJB.

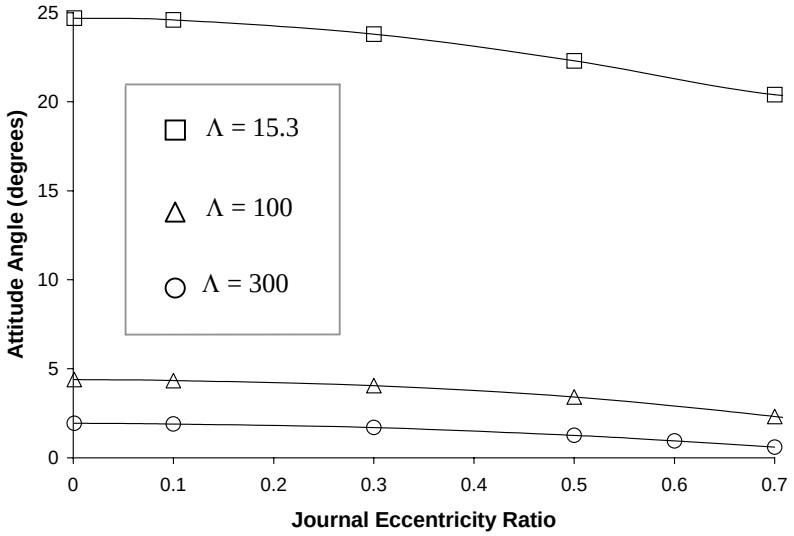

Figure (8). Journal attitude angles versus eccentricity ratio for a gas HGJB.

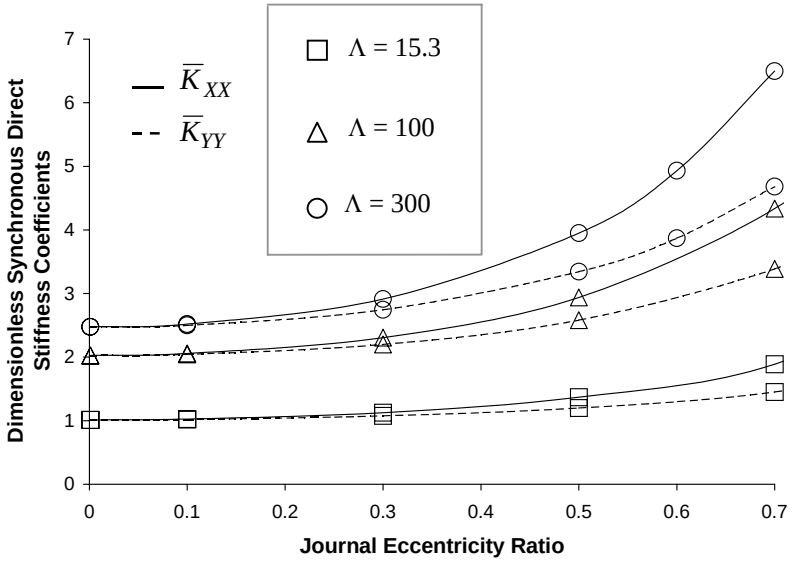

Figure (9). Dimensionless synchronous direct stiffness coefficients versus eccentricity ratio for a gas HGJB.

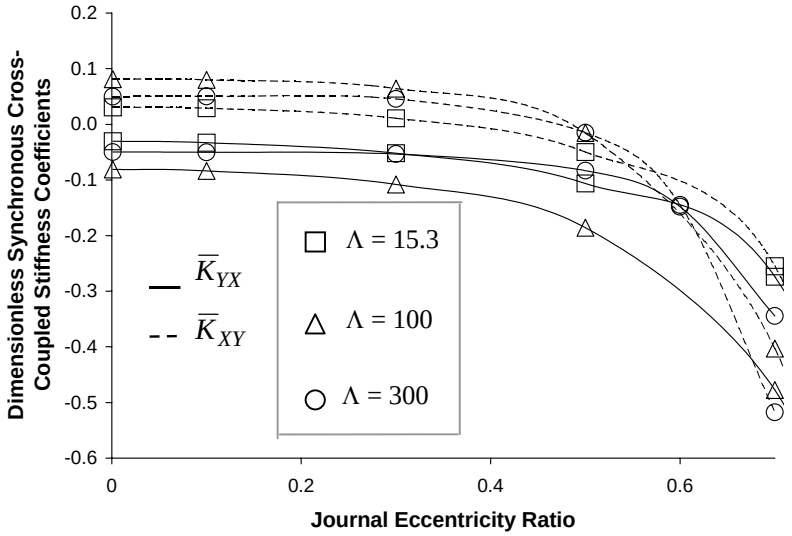

Figure (10). Dimensionless synchronous cross-coupled stiffness coefficients versus eccentricity ratio for a gas HGJB.

8. Conclusions

An efficient and accurate finite element procedure is implemented to analyze the behavior of gas lubricated herringbone groove journal bearings (HGJBs). This procedure is based on the Galerkin weighted residual method with a new class of high-order shape functions, which are derived from the non-linear Reynolds equation for compressible fluids within an element domain. The implemented finite element procedure is capable of rendering accurate predictions of some static and dynamic performance characteristics of high speed gas HGJBs. Curves of some performance characteristics, such as bearing load capacity and dynamic force coefficients, versus operating parameters show the influence of high speeds on the behavior of gas HGJBs operating at concentric and eccentric journal positions. The finite element analysis is carried out for bearings with rotating smooth journal at small, medium and large eccentricity ratios. This work shows that the bearing load capacity and dynamic force coefficients tend to asymptotic values as the journal rotating speed increases.

9. References

Bathe, K.J., 1982, "Finite Element Procedures in Engineering Analysis", Prentice-Hall, Englewood Cliffs, NJ, USA.

Bonneau, D. and Absi, J., 1994, "Analysis of Aerodynamic Journal Bearings with Small Number of Herringbone Grooves by Finite Element Method", ASME Journal of Tribology, Vol. 116, pp. 698-704.

Constantinescu, V.N. and Dimofte, F., 1987, "On the Influence of the Mach Number on Pressure Distribution in Gas Lubricated Step Bearings", Revue Roumaine des Sciences Techniques, Tome 32, No. 1, pp. 51-66.

Cunningham, R.E., Fleming, D.P. and Anderson, W.J., 1969, "Experimental Stability Studies of the Herringbone-Grooved Gas-Lubricated Journal Bearing", ASME Journal of Lubrication Technology, pp.52-59.

Dahlquist, G. and Björck, A., 1974, "Numerical Methods", Prentice-Hall, Englewood Cliffs, NJ, USA.

Dimofte, F. and Keith, T.G. Jr., 1998, "Wave Bearing Technology to Control Journal Bearing Dynamics", Proceedings of the 7th International Symposium on Transport Phenomena and Dynamics of Rotating Machinery (ISROMAC), Honolulu, Hawaii, USA. Vol. A, pp. 327-336.

Faria, M.T.C., 1999, "A Novel Finite Element Procedure for Hydrodynamic Thin Gas Film Lubrication", Proceedings of the 15th Brazilian Congress of Mechanical Engineering, Águas de Lindóia, Brazil, pp. 1-10.

Faria, M.T.C. and San Andrés, L., 2000, "On the Numerical Modeling of High-Speed Hydrodynamic Gas Bearings", ASME Journal of Tribology, Vol. 122, No. 1, pp. 124-130.

Faria, M.T.C., 2001, "Some Performance Characteristics of High Speed Gas Lubricated Herringbone Groove Journal Bearings", JSME International Journal, Ser. C, Vol. 44, N0. 3, pp. 775-781.

Hamrock, B.J., 1994, "Fundamentals of Fluid Film Lubrication", McGraw-Hill, New York, USA.

Kinouchi, K., Tanaka, K., Yoshimura, S. and Yagawa, G., 1996, "Finite Element Analysis of Gas-Lubricated Grooved Journal Bearings (Analysis Method)", JSME International Journal, Ser. C, Vol. 39, No. 1, pp.123-129.

Pan, C.H.T., 1990, "Gas Lubrication (1915-1990)", Achievements in Tribology, ASME Publication, pp.31-55.

van der Stegen, R.H.M., 1997, "Numerical Modelling of Self-Acting Gas Lubricated Bearings with Experimental Verification", Ph.D. Dissertation, The University of Twente, The Netherlands.